

# Squeeze-out of nuclear matter in peripheral heavy-ion collisions and momentum-dependent effective interactions. \*

A.B. Larionov <sup>†</sup>, W. Cassing, C. Greiner, U. Mosel

*Institut für Theoretische Physik, Universität Giessen, D-35392 Giessen, Germany*

## Abstract

We perform a systematic study of in-plane and out-of-plane proton and neutron flow from nucleus-nucleus collisions within the BUU transport approach employing different parameter sets for the mean-field potentials that can be characterized by the nuclear incompressibility and the stiffness of the momentum-dependent potential. We find that a simultaneous description of the experimental data from the BEVALAC and the SIS on both the nucleon squeeze-out  $v_2$  and the in-plane flow  $F$  at beam energies  $E_{lab} = 0.15 \div 2$  AGeV requires a mean field with strong momentum dependence, i.e. an effective Landau mass  $m^* \simeq 0.68m_0$  at normal nuclear matter density  $\rho_0 = 0.17$  fm<sup>-3</sup>, where  $m_0 = 0.938$  GeV is the bare nucleon mass. Some experimental data on the squeeze-out require an even stiffer momentum dependence ( $m^* \approx 0.62 m_0$ ). All systems investigated are found to be compatible with  $m^*/m_0 = 0.65 \pm 0.03$ .

PACS numbers: 25.70.-z; 25.75.-q; 25.75.Ld; 21.65.+f

*Keywords:* Heavy-ion collisions; Collective flow; Transport models; Equation of state; Effective mass

---

\*Supported by BMBF and GSI Darmstadt

<sup>†</sup>On leave from RRC "I.V. Kurchatov Institute", 123182 Moscow, Russia

## I. INTRODUCTION

Since many years the study of the various collective flows of nuclear matter is one of the main subjects in heavy-ion physics [1–4] aiming to extract the equation of state (EOS) of nuclear matter. It was shown in Refs. [5–8], that the in-plane directed flow [9] is sensitive to both the incompressibility  $K$  of the EOS and to the momentum-dependent effective interaction (MDI). Moreover, the in-medium nucleon-nucleon (NN) cross section also influences the transverse directed flow [10] since nucleons achieve transverse momentum also by elastic and inelastic collisions. It is necessary, therefore, to have at least two additional observables, besides in-plane flow, in order to determine three most commonly used components of the effective NN interaction adopted in the various analyses: the  $K$ -value, the stiffness of MDI and, possibly, the in-medium NN cross section.

The rapidity distribution of nucleons, which is only weakly dependent on the mean-field parameters, gives reasonable constraints on the in-medium NN cross section or on the nuclear stopping power [11,12]. However, it was not so clear until recently, how to possibly extract information on the MDI from heavy-ion collisions. Danielewicz [13] has shown within the Boltzmann-Uehling-Uhlenbeck (BUU) transport model, that the elliptic flow (or squeeze-out ratio) of protons at midrapidity is very sensitive to the MDI part of the nucleon mean field. The reaction Bi+Bi at  $E_{lab}=400, 700, 1000$  AMeV (measured by the KAOS Collaboration [14]) has been analysed in [13] leading to the conclusion that the MDI part of the NN interaction should produce an effective Landau mass  $m^* \simeq 0.7m_0$ , since momentum independent forces ( $m^* = m_0$ ) strongly underpredict the squeeze-out ratio at high transverse momenta [13].

The aim of our present work is: (i) to study the mechanism of the squeeze-out enhancement by the MDI and (ii) to analyse several independent data sets on the *directed* and *elliptic* flow of nucleons to get experimental constraints on the stiffness of the MDI.

The paper is structured as follows: In Sect. II a brief description of the applied BUU model is given. Sect. III contains our interpretation underlying the squeeze-out mechanism,

which is illustrated in Sect. IV by a detailed study of the time evolution of colliding nuclear systems within BUU. A comparison to the experimental data on the proton and neutron elliptic and directed flows is given in Sect. V, while Sect. VI concludes our work with a summary of the results.

## II. THE BUU MODEL

In our calculations we have applied the recent version of the BUU model described in detail in Ref. [15]. The equation of motion for the nucleon phase-space distribution function  $f(\mathbf{r}, \mathbf{p}, t)$  includes a propagation in the momentum-dependent scalar mean field  $s(\mathbf{r}, \mathbf{p}, f)$  via the single-particle energy

$$H_{mf}(\mathbf{r}, \mathbf{p}, t) = \sqrt{(m_0 + s(\mathbf{r}, \mathbf{p}, f))^2 + p^2} . \quad (1)$$

Both elastic and inelastic scattering processes are additionally described by the r.h.s. of the transport equation

$$\begin{aligned} & \left( \frac{\partial}{\partial t} + \frac{\partial H_{mf}}{\partial \mathbf{p}_1} \frac{\partial}{\partial \mathbf{r}} - \frac{\partial(H_{mf} + U_{Coul})}{\partial \mathbf{r}} \frac{\partial}{\partial \mathbf{p}_1} \right) f(\mathbf{r}, \mathbf{p}_1, t) \\ &= \int \frac{g d\mathbf{p}_2}{(2\pi\hbar)^3} \int d\Omega v_{12} \frac{d\sigma_{NN}(p_{12})}{d\Omega} (f_3 f_4 (1 - f_1)(1 - f_2) - f_1 f_2 (1 - f_3)(1 - f_4)) \\ &+ \text{coupling terms} , \end{aligned} \quad (2)$$

where  $U_{Coul}$  is the Coulomb potential acting on protons;  $g = 4$  is the spin-isospin degeneracy of a nucleon;  $v_{12} = |\mathbf{v}_1 - \mathbf{v}_2|$  and  $p_{12} = |\mathbf{p}_1 - \mathbf{p}_2|$  are the relative velocity and relative momentum of colliding nucleons, respectively;  $d\sigma_{NN}(p_{12})/d\Omega$  is the energy dependent differential NN scattering cross section as parametrized by Cugnon [16];  $f_i := f(\mathbf{r}, \mathbf{p}_i, t)$  ( $i = 1, 2, 3, 4$ ), while  $\mathbf{p}_3$  and  $\mathbf{p}_4$  are the final momenta of the scattered nucleons. The coupling terms in (2) account for the various inelastic channels:  $NN \Leftrightarrow \pi NN$ ,  $NN \Leftrightarrow NR$  – S-wave pion and resonance production/absorption,  $NN \rightarrow \Lambda KN$ ,  $NN \rightarrow \Sigma^0 KN$  – strangeness production.

The scalar potential  $s(\mathbf{r}, \mathbf{p}, f)$  is computed as follows (see [17]): 1) In the local rest frame (l.r.f.) of the nuclear matter element, where the space components of the baryonic 4-current  $j^\mu = (j^0, \mathbf{j})$  vanish, i.e.  $\mathbf{j} = 0$ , the single-particle energy is calculated as

$$\epsilon_{l.r.f.}(\mathbf{r}, \mathbf{p}) = \sqrt{m_0^2 + p^2} + U(\rho, \mathbf{p}) . \quad (3)$$

The explicit form of the momentum-dependent potential  $U$  in (3) is taken from [18] as

$$U(\rho, \mathbf{p}) = A \frac{\rho}{\rho_0} + B \left( \frac{\rho}{\rho_0} \right)^\tau + \frac{2C}{\rho_0} \int \frac{gd\mathbf{p}'}{(2\pi\hbar)^3} \frac{f(\mathbf{r}, \mathbf{p}')}{1 + (\mathbf{p} - \mathbf{p}')^2/\Lambda^2} . \quad (4)$$

A symmetry energy term is not taken into account in the potential (4). 2) The mean field  $s$  is found from the relation in the l.r.f.

$$s = \sqrt{\epsilon_{l.r.f.}^2 - p^2} - m_0 . \quad (5)$$

3) The scalar potential  $s$  is then used in Eq. (1) to determine the single-particle energy in the computational frame. Steps 1)-3) are repeated until selfconsistency is reached, i.e.  $s$  is not changed within the accuracy of numerics on the level of  $10^{-4}$ .

The interaction range  $\Lambda$  of the potential (4) is chosen as in Ref. [18]:  $\Lambda = 1.5p_F^{(0)}$ , where  $p_F^{(0)} \equiv p_F(\rho_0)$ ,  $p_F(\rho) = (\frac{3}{2}\pi^2\rho)^{1/3}\hbar$ . The residual four free parameters  $A$ ,  $B$ ,  $\tau$  and  $C$  of the potential  $U$  are determined from the conditions:

(i) The effective mass at the Fermi surface

$$(m^*)^{-1} = m_0^{-1} + (p_F^{(0)})^{-1} \frac{\partial U}{\partial p} \Big|_{p=p_F^{(0)}} \quad (6)$$

must be in the range  $0.6m_0 \leq m^* \leq m_0$  (c.f. [19,20]). This condition puts limits on the stiffness  $C$  of the MDI.

(ii) The energy per nucleon in nuclear matter has a minimum at  $\rho = \rho_0$  and

(iii) has a value of  $-16$  MeV at minimum:

$$\frac{\partial \epsilon/\rho}{\partial \rho} \Big|_{\rho=\rho_0} = 0 , \quad \frac{\epsilon}{\rho} \Big|_{\rho=\rho_0} = -16 \text{ MeV} , \quad (7)$$

where

$$\begin{aligned} \epsilon(\rho) = & \frac{3}{5}\epsilon_F\rho + \frac{1}{2}A\frac{\rho^2}{\rho_0} + \frac{1}{\tau+1}B\frac{\rho^{\tau+1}}{\rho_0^\tau} + \\ & \frac{C}{\rho_0} \int \frac{gd\mathbf{p}_1}{(2\pi\hbar)^3} \frac{gd\mathbf{p}_2}{(2\pi\hbar)^3} \frac{f(\mathbf{p}_1)f(\mathbf{p}_2)}{1 + (\mathbf{p}_1 - \mathbf{p}_2)^2/\Lambda^2} \end{aligned} \quad (8)$$

with  $\epsilon_F = p_F^2/2m_0$  and  $f(\mathbf{p}) = \Theta(p_F - p)$ . Explicit forms of the momentum integrals in (6),(8) are given in Ref. [18].

(iv) The nuclear matter incompressibility

$$K = 9\rho_0^2 \frac{\partial^2 \epsilon / \rho}{\partial \rho^2} \Big|_{\rho=\rho_0} \quad (9)$$

is fitted in the range  $K = 200 \div 380$  MeV.

We have applied in our calculations the following mean fields denoted by H (hard, without momentum dependence), HM and SM (hard and soft, with a "standard" momentum dependence) as well as the new mean field parametrization which is dubbed HM1 (see below). The parameters of all interactions are presented in Table 1. The stiffness  $C$  of the MDI in the interactions HM and SM is close to that of Ref. [18]. The set of parameters HM1 includes an MDI stiffness that is about 30% larger than in HM and SM, which leads to a smaller effective mass at the Fermi momentum for HM1. In Fig. 1 we show the resulting energy per nucleon as a function of density and the potential  $U(\rho, p)$  versus momentum for several densities. The interactions H, HM and HM1 give practically the same EOS ( $E/A(\rho)$ -dependence), but they differ in the MDI part, i.e. in their momentum dependence. This gives the possibility to extract an independent information on the MDI stiffness  $C$ . On the other hand, the interactions HM and SM produce different EOS, but have the same MDI, which is relevant for a separate study on the sensitivity to the incompressibility  $K$ .

### III. SQUEEZE-OUT MECHANISM

Squeeze-out of nucleons is observed in the beam energy range below  $1 \div 2$  AGeV where mean field effects still play an essential role. It can be interpreted, however, to a major extent in terms of a shadowing phenomenon [21], as in the participant-spectator picture of a heavy-ion collision the fireball particles – emitted in the reaction plane – are rescattered on the spectators. This results intuitively in a squeeze-out ratio  $R_N := (N(90^\circ) + N(270^\circ))/(N(0^\circ) + N(180^\circ))$  at midrapidity being larger than 1. Here  $N(\phi)$

is the azimuthal distribution of nucleons with respect to the reaction plane in a given rapidity interval. A specific particle emitted from the center-of-mass of a system and moving in transverse direction with velocity  $v_t$  will be shadowed by the spectator piece, if it reaches the spectator during the passage time  $\Delta t = 2R/(v_p^{c.m.}\gamma)$  of the colliding nuclei. Here  $R$  is the radius of the nuclei (assumed to be equal for projectile and target),  $v_p^{c.m.}$  is the projectile velocity in the center-of-mass system, and  $\gamma = (\sqrt{1 - (v_p^{c.m.})^2})^{-1}$ . A straightforward geometrical estimate then leads to the condition  $v_t\Delta t/2 > R - b/2$ , or

$$v_t > \frac{R - b/2}{R} \gamma v_p^{c.m.}, \quad (10)$$

where  $b$  is the impact parameter. One can see from (10) that at larger impact parameters  $b$  the lower limit of  $v_t$  becomes smaller, i.e. more particles will be shadowed and the squeeze-out ratio  $R_N$  will become larger (c.f. later Fig. 11). This is simply related to a larger size  $\sim b$  of the spectator pieces in peripheral collisions. It is also evident, that for faster moving particles it is easier to fulfill the condition (10) and, therefore, the squeeze-out ratio should grow with the particle transverse velocity  $v_t$  (c.f. later Figs. 6,12).

The squeeze-out phenomenon can also be characterized by a negative elliptic flow  $v_2$  (c.f. [22]) which appears in the Fourier expansion

$$N(\phi) \propto 1 + 2v_1 \cos(\phi) + 2v_2 \cos(2\phi) + \dots \quad (11)$$

Neglecting thus higher order terms in (11), the following direct relation is obtained:

$$R_N \simeq \frac{1 - 2v_2}{1 + 2v_2}. \quad (12)$$

In (11) the elliptic flow  $v_2$  is given as

$$v_2 = \left\langle \frac{p_x^2 - p_y^2}{p_x^2 + p_y^2} \right\rangle. \quad (13)$$

At higher beam energy ( $\sim 10$  AGeV), faster moving and Lorentz-contracted spectators do not shadow particles any more from the expanding fireball. This results in  $R_N \leq 1$  (or  $v_2 \geq 0$ ) as observed in experiment [23].

The simple geometrical picture discussed above will be illustrated by the study of the BUU phase-space evolution in the next section. Since the squeeze-out is related to the participant-spectator reaction mechanism (c.f. [24]), we expect a lower beam-energy limit of  $\sim 0.1$  AGeV for  $R_N > 1$ . At even lower beam energies the mean-field effects lead to the formation of rotating nuclear systems [25] that emit particles mostly in the reaction plane due to centrifugal forces and thus producing  $R_N < 1$  (or  $v_2 > 0$ , c.f. later Fig. 7).

#### IV. BUU STUDY OF THE SQUEEZE-OUT TIME EVOLUTION

We study the system Au+Au at the beam energy  $E_{lab} = 0.4$  AGeV and impact parameter  $b = 6$  fm. Fig. 2 shows the time evolution of the central baryon density and of the NN collision rate for the HM and SM mean fields. In agreement to Fig. 1 (upper left panel), a slightly higher density and, as a consequence, a higher collision rate are reached in the case of the SM parametrization. However, the various EOS shown in Fig. 1 practically do not differ in the density interval  $0 < \rho \leq 0.27 \text{ fm}^{-3}$  probed in the collision. We do not expect, therefore, to get clear constraints on the incompressibility  $K$  from our study of the *peripheral* collisions concentrating mainly on the MDI-part of the effective interactions.

As pointed out in Ref. [13] the  $p_t$ -dependence of the  $v_2$  coefficient is very sensitive to the momentum dependence of the nuclear mean field. In order to understand this fact, we have performed calculations with the parametrizations H and HM of the mean field. Fig. 3 shows the average transverse velocity (a) and transverse momentum (b) of the midrapidity neutrons moving in- and out- of the reaction plane versus time. We observe that in the case of the HM parameterset  $\langle v_t \rangle$  reaches a maximum at  $t \simeq 17$  fm/c when also the central density and the collision rate are close to the maximum (Fig. 2). At this time the system shows the most compact configuration in space, i.e. the line connecting the centers of target and projectile spectators, is perpendicular to the beam ( $z$ -) direction (Fig. 4). However, in case of the H mean field the transverse velocity does not have a maximum (the peaks of  $\langle v_t \rangle$  and  $\langle p_t \rangle$  at  $t \simeq 7$  fm/c are due to fluctuations, because initially there are no nucleons

at midrapidity). Moreover, at  $t < 40$  fm/c in the case of the HM mean field the average transverse velocity is larger than for the mean field H, while the transverse momentum is practically independent on the mean field, even showing a slightly opposite tendency: at  $t < 40$  fm/c the mean field H produces a somewhat larger  $\langle p_t \rangle$ . This can be qualitatively understood from the Hamiltonian equations:

$$\dot{\mathbf{r}} = \frac{\partial H_{mf}}{\partial \mathbf{p}} = \frac{\mathbf{p}}{H_{mf}} + \frac{m_0 + s}{H_{mf}} \frac{\partial s}{\partial \mathbf{p}}, \quad (14)$$

$$\dot{\mathbf{p}} = -\frac{m_0 + s}{H_{mf}} \frac{\partial s}{\partial \mathbf{r}}. \quad (15)$$

where  $H_{mf}$  is the single-particle energy (1). For the momentum-independent H field, (14) reduces to a simple proportionality:  $\mathbf{v} = \mathbf{p}/H_{mf}$ , where  $H_{mf} \sim 1$  GeV. However, for the HM interaction the strong momentum-dependent mean field  $s(\mathbf{r}, \mathbf{p}, f)$  is created by the density build-up, and the second term in the r.h.s. of (14) becomes large (and positive), which results in a larger transverse velocity for HM. On the other hand, the force acting on a particle depends mostly on the EOS produced by a given mean field or on the pressure gradient. Thus, the r.h.s. of (15) depends relatively weakly on the momentum dependence of a mean field.

Later on  $\langle v_t \rangle$  and  $\langle p_t \rangle$  decrease reaching asymptotic values at  $t \simeq 50$  fm/c. This decrease is due to less energetic products of NN scattering, which populate the midrapidity region at later times, while first-chance collision products have larger kinetic energies. Faster moving particles (in the case of the HM calculation with respect to H) are shadowed more effectively, which causes a larger splitting between in- and out-of-plane transverse velocities for the HM calculation at large times.

In Fig. 5 we show the final azimuthal angle dependence of the midrapidity neutron transverse velocity (a) and the neutron azimuthal distribution (b). The azimuthal angle modulation of the transverse velocity is clearly visible, which was first observed experimentally [26]. The transverse velocity azimuthal angle dependence and the azimuthal distribution of particles have the same shape. The depletion of the particle yield at  $\phi = 0^\circ$  and  $180^\circ$  is caused by a shadowing of fast moving particles by the spectators; the enhanced yield at

$\phi = \pm 90^\circ$  correlates with a nonshadowed emission of fast particles.

Fig. 6 shows the  $v_2$ -coefficient vs. transverse velocity (left panels) and vs. transverse momentum (right panels) at the two time steps  $t = 30$  fm/c and  $t = 50$  fm/c. Even at 30 fm/c the particles still feel the influence of the nuclear field and, therefore, the simple relation  $v_t = p_t/H_{mf}$  can be applied at this moment only in the case of the momentum-independent mean field H. One can see, that at 30 fm/c the  $v_2(p_t)$ -dependence is different for different mean fields, while the  $v_2(v_t)$ -dependence is very similar for the H and HM calculations. This is in agreement with our expectation, that particles moving with the same transverse velocity are shadowed in the same way regardless of their transverse momenta. At later times, this "transient universality" of  $v_2(v_t)$  is destroyed since the influence of the mean field will become negligible here and  $v_t = p_t/\sqrt{m_0^2 + p^2}$  for both parametersets.

## V. COMPARISON WITH EXPERIMENT

In our comparison to data on squeeze-out observables we now compare in parallel also to data on the in-plane flow  $F$ , which is defined as the derivative of the transverse in-plane momentum component  $\langle p_x \rangle$  with respect to the normalized rapidity  $y^{(0)} = (y/y_{proj})_{c.m.}$  at midrapidity [27]:

$$F = \frac{d\langle p_x \rangle}{dy^{(0)}|_{y^{(0)}=0}}. \quad (16)$$

A simultaneous description of both observables, i.e.  $v_2$  and  $F$ , will give a rather strong confidence that the dynamics of the participant zone and the interaction of the participating nucleons with the spectators are described consistently in our calculation and potentially leading to stringent constraints on the EOS and the interactions employed (see also [28] where the energy regim below 100 AMeV has been studied).

Figs. 7 and 8 show the excitation functions of  $v_2$  and  $F$  for protons in case of Au+Au collisions at the beam energies  $E_{lab}=0.05, 0.15, 0.25, 0.4, 0.6, 0.8, 1.06$  and 2 AGeV in the impact parameter range  $b = 5 \div 7$  fm corresponding to an estimate given in Refs. [23,29].

The data are taken from Refs. [30,31]. The time evolution has been followed until  $t_{max}=200$  fm/c at  $E_{lab}=0.05$  AGeV, 150 fm/c at  $0.15 \div 0.6$  AGeV, 100 fm/c at 0.8 AGeV, 50 fm/c at 1.06 AGeV and 40 fm/c at 2 AGeV. Free protons were selected by the requirement, that the distance to the closest particle within a given parallel ensemble is more than some critical distance  $d_c \simeq 3$  fm in order to separate from protons bound in fragments.

The  $v_2$  coefficient was calculated for protons in the c.m. rapidity range  $|y| < 0.1$ . As discussed in Sect. III, the elliptic flow  $v_2$  vs.  $E_{lab}$  shows a nonmonotonic behaviour: it decreases from positive to negative values reaching a minimum at  $E_{lab} \simeq 0.4$  AGeV, and then it starts to increase moderately again with beam energy. In this work, however, we only concentrate on the beam energy domain below 2 AGeV and, therefore, the transition from negative to positive  $v_2$  at a beam energy  $\sim 4$  AGeV [23,32] is not discussed here. The lower transition energy, i.e. the beam energy at which  $v_2$  changes sign [33], is  $E_{TRA} \simeq 100$  AMeV. The in-plane flow increases monotonically in the beam energy region considered. The calculated balance energy, i.e. the beam energy at which the flow  $F$  changes sign, is  $E_{BAL} \simeq 60$  AMeV. These values of  $E_{TRA}$  and  $E_{BAL}$  are in agreement with the FOPI-data from Ref. [33].

Now we will discuss the effects of various mean field properties and of the NN cross section on  $v_2$  and  $F$ . The calculation with a momentum-independent mean field H fails to reproduce the strong squeeze-out at  $E_{lab} \simeq 0.4$  AGeV (Fig. 7) and also underpredicts the flow  $F$  in the energy regime  $E_{lab} = 0.15 \div 2$  AGeV (Fig. 8). The HM parametrization increases the in-plane flow and squeeze-out (see also Fig. 5) and, thus, improves the agreement with both observables, however, a tendency to underpredict the in-plane flow  $F$  is still present. The lower incompressibility  $K$  in the SM calculation results in a reduced squeeze-out and a reduced flow with respect to the HM calculation. The in-plane flow data are underpredicted in the case of the SM mean field at  $E_{lab} \leq 250$  AMeV and at  $E_{lab} \geq 800$  AMeV.

We achieve a satisfactory description of the in-plane flow excitation function only by employing the mean field HM1 with a 30% increased MDI stiffness C and an incompressibility  $K = 380$  MeV. On the other hand, the squeeze-out  $v_2$  becomes a little bit too strong in

the case of HM1. As known from Ref. [25], a reduction of the NN cross section improves the agreement of the BUU calculation with the data on the squeeze-out for Au+Au at  $E_{lab} = 100 \div 250$  AMeV. We also see from Fig. 7, that a 30% reduction of the NN cross-section decreases the squeeze-out giving a somewhat better overall agreement with the data on  $v_2$ . The reason for this behaviour is the larger mean-free-path of particles and, therefore, a reduced shadowing by spectators. Though a slightly better agreement of the calculation with a reduced NN cross section is achieved for the  $v_2$ -data, we now underestimate the in-plane flow (Fig. 8). Generally, one can observe from Figs. 7 and 8, that the mean field HM gives the best overall agreement with the data on the excitation functions of  $v_2$  and  $F$ .

In Fig. 9 we present the midrapidity neutron azimuthal distributions with respect to the in-plane flow axis for the reactions Nb+Nb and La+La at 400 AMeV in comparison to the data from Ref. [34] (see Fig. 11 of [34]). In this comparison the BUU events were treated as the experimental data [34], i.e. the azimuthal angle of the reaction plane was defined by the  $\mathbf{Q}$  vector:

$$\mathbf{Q} = \sum_{\nu} w^{\nu} \frac{\mathbf{v}_t^{\nu}}{|\mathbf{v}_t^{\nu}|}, \quad (17)$$

where the sum is taken over all charged fragments (i.e. all protons in BUU);  $\mathbf{v}_t^{\nu}$  is the transverse velocity of the particle  $\nu$ ;  $w^{\nu} = 1$  for  $y^{(0)} \geq 0.2$ ,  $w^{\nu} = 0$  for  $-0.2 \leq y^{(0)} \leq 0.2$ ,  $w^{\nu} = -1$  for  $y^{(0)} < -0.2$ . Furthermore, we have determined the flow angle  $\Theta_F$  by diagonalizing the flow tensor  $F_{ij}$  in the c.m.s. (see [35]):

$$F_{ij} = \sum_{\nu} \frac{1}{2m_0} \frac{v_i^{\nu} v_j^{\nu}}{|\mathbf{v}^{\nu}|^2}. \quad (18)$$

Finally, a rotation of the c.m. coordinate system was performed, first, around the beam z-axis to align the x-axis with the vector  $\mathbf{Q}$  and, second, around the y-axis by the flow angle  $\Theta_F$  (see [36]). As shown in Ref. [36], the squeeze-out is more pronounced in the rotated coordinate system  $(x', y', z')$ . The azimuthal distributions in Fig. 9 are presented for neutrons with longitudinal momenta  $-0.1 \leq (p'_z/p'_{proj})_{c.m.} \leq 0.1$ . We see from Fig. 9, that the data can be reasonably well reproduced adopting the HM1 mean field, suggesting

that the MDI stiffness  $C$  in the parameterset HM is not high enough. Our conclusion is in line with results of [34], where it was reported that BUU calculations with the mean field of [18] ( $K = 215$  MeV, i.e. the SM parametrization) underpredict the squeeze-out.

Fig. 10 shows the in-plane transverse momentum  $\langle p_x \rangle$  of neutrons versus the normalized rapidity  $y^{(0)}$  for the reactions Nb+Nb and La+La at 400 AMeV. We observe that an increased MDI stiffness improves the agreement with the neutron in-plane flow data, too.

Finally, we have studied the neutron squeeze-out in Au+Au collisions measured by the FOPI-LAND Collaboration [37]. Fig. 11 shows the impact parameter dependence of the squeeze-out ratio  $R_N$  for Au+Au collisions at 400 AMeV, which reasonably describes the data for the HM calculation (dotted histogram). The HM1 parameterset (solid histogram) underpredicts somewhat the squeeze-out ratio in central collisions and overpredicts it in semiperipheral ( $b = 7 \div 8$  fm) collisions. The SM parameterset (dash-dotted histogram) and momentum-independent field H (dashed histogram) underpredict the data at large impact parameters. The calculated  $R_N(b)$ -dependence has a characteristic bell-shape with a maximum at  $b \simeq 7$  fm. This agrees with the results of Ref. [33], where the squeeze-out was studied for charged particles. The drop of  $R_N$  at large impact parameters can be explained by a smaller compression of the participant zone and, therefore, smaller transverse velocities of particles emitted in peripheral collisions.

In Fig. 12 the  $p_t$ -dependence of the ratio  $R_N$  is shown for collisions of Au+Au at 400, 600 and 800 AMeV. In agreement with previous calculations of Ref. [13], we observe that a lower effective mass, i.e. a steeper momentum dependence, increases the squeeze-out ratio  $R_N$  at large  $p_t$  (c.f. dotted and solid lines on Fig. 12 d-f). On the other hand, reducing the NN cross section decreases the ratio  $R_N$  at large  $p_t$  (c.f. solid and long-dashed lines on Fig. 12 e). The parameterset H produces too flat  $R_N(p_t)$ -dependence (c.f. short-dashed line on Fig. 12 a). The SM calculation gives the best overall agreement with the data (dash-dotted line on Fig. 12 a-c). We see that our BUU calculations reproduce the experimentally observed trend of  $R_N$  to decrease at fixed  $p_t$  with collision energy, which was interpreted in Ref. [37] as a scaling behaviour of the squeeze-out.

## VI. SUMMARY AND CONCLUSIONS

The squeeze-out of nuclear matter in heavy-ion collisions at beam energies  $E_{lab} = 0.05 \div 2$  AGeV has been studied within the BUU approach of Ref. [15]. As demonstrated, being essentially caused by the shadowing of the expanding fireball by cold spectators, the squeeze-out is quite sensitive to the specific velocity of the particles. A mean field with a larger MDI stiffness gives a smaller effective mass, and thus a harder velocity spectrum of nucleons. In an ongoing heavy-ion collision faster moving nucleons are subsequently shadowed more effectively and the squeeze-out ratio  $R_N$  is larger for mean fields with stronger momentum dependence.

The systematic comparison with the experimental data on the excitation function of the elliptic flow  $v_2$  [30] favours mean fields with  $m^* \simeq 0.68m_0$ , i.e. HM or SM sets. The influence of the incompressibility  $K$  on the squeeze-out turns out to be quite weak. At the same time, a reproduction of the in-plane flow data of the FOPI and EOS Collaborations on Au+Au collisions at 150 and 250 AMeV [31] requires an enhanced MDI stiffness (HM1 parameterset:  $K = 379$  MeV and  $m^* = 0.62m_0$ ). Further evidence for an increased MDI stiffness (at  $p < 1$  GeV/c) is obtained from a comparison with the BERKELEY data [34] on the neutron azimuthal distributions and the in-plane flow in Nb+Nb and La+La collisions at 400 AMeV. However, the FOPI-LAND data [37] on the neutron squeeze-out in Au+Au collisions at  $400 \div 800$  AMeV favour the standard MDI stiffness (HM or SM parametersets).

To conclude, a simultaneous description of the nucleon squeeze-out  $v_2$  and the in-plane flow  $F$  at the beam energies  $E_{lab} = 0.15 \div 2$  AGeV requires a mean field with a strong momentum dependence. This corresponds to the effective Landau mass at the Fermi surface  $m^*/m_0 = 0.65 \pm 0.03$  at normal nuclear density. The incompressibility  $K$ , however, is less well determined since in semiperipheral reactions the average density probed up to 1 AGeV is too low.

## REFERENCES

- [1] W. Scheid, R. Ligensa, and W. Greiner, Phys. Rev. Lett. **21**, 1479 (1968)
- [2] H. Stöcker and W. Greiner, Phys. Rep. **137**, 277 (1986)
- [3] P.K. Sahu, A. Hombach, W. Cassing, M. Effenberger, U. Mosel, Nucl. Phys. A **640**, 493 (1998)
- [4] A. Hombach, W. Cassing, S. Teis and U. Mosel, Eur. Phys. J. A **5**, 157 (1999)
- [5] C. Gale, G. Bertsch, S. Das Gupta, Phys. Rev. C **35**, 1666 (1987)
- [6] J. Aichelin, A. Rosenhauer, G. Peilert, H. Stöcker, and W. Greiner, Phys. Rev. Lett. **58**, 1926 (1987)
- [7] C. Gale, G.M. Welke, M. Prakash, S.J. Lee, and S. Das Gupta, Phys. Rev. C **41**, 1545 (1990)
- [8] J. Zhang, S. Das Gupta, and C. Gale, Phys. Rev. C **50**, 1617 (1994)
- [9] P. Danielewicz and G. Odyniec, Phys. Lett. B **157**, 146 (1985)
- [10] H.M. Xu, Phys. Rev. Lett. **67**, 2769 (1992); Phys. Rev. C **46**, R392 (1992)
- [11] V.N. Russkikh, Yu.B. Ivanov, Yu.E. Pokrovsky, P.A. Henning, Nucl. Phys. A **572**, 749 (1994)
- [12] A. Hombach, W. Cassing, and U. Mosel, Eur. Phys. J. A **5**, 77 (1999)
- [13] P. Danielewicz, nucl-th/9912027, Nucl. Phys. A, in press
- [14] D. Brill et al., Z. Phys. A **355**, 61 (1996)
- [15] M. Effenberger, E.L. Bratkovskaya, and U. Mosel, Phys. Rev. C **60**, 044614 (1999)
- [16] J. Cugnon, D. L'Hôte, J. Vandermeulen, Nucl. Instr. and Meth. B **111**, 215 (1996)
- [17] S. Teis, W. Cassing, M. Effenberger, A. Hombach, U. Mosel, and G. Wolf, Z. Phys. A

- 356**, 421 (1997)
- [18] G.M. Welke, M. Prakash, T.T.S. Kuo, S. Das Gupta, and C. Gale, Phys. Rev. C **38**, 2101 (1988)
- [19] M. Prakash et al., Phys. Rep. **280**, 1 (1997)
- [20] E. Chabanat et al., Nucl. Phys. A **627**, 710 (1997)
- [21] J. Aichelin, Phys. Rep. **202**, 233 (1991)
- [22] H. Appelshäuser et al. (NA49 Collaboration), Phys. Rev. Lett. **80**, 4136 (1998)
- [23] C. Pinkenburg et al. (E895 Collaboration), Phys. Rev. Lett. **83**, 1295 (1999)
- [24] J. Gosset et al., Phys. Rev. C **16**, 629 (1977)
- [25] M.B. Tsang et al., Phys. Rev. C **53**, 1959 (1996)
- [26] G. Rai, Equation of State Workshop, GSI, Darmstadt, February 20-23, unpublished
- [27] K.G.R. Doss et al., Phys. Rev. Lett. **57**, 302 (1986)
- [28] Yu-Ming Zheng, C.M. Ko, Bao-An Li, and Bin Zhang, Phys. Rev. Lett. **83**, 2534 (1999)
- [29] M.D. Partlan et al. (EOS Collaboration), Phys. Rev. Lett. **75**, 2100 (1995)
- [30] N. Herrmann, J.P. Wessels, and T. Wienold, Annu. Rev. Nucl. Part. Sci. **49**, 581 (1999)
- [31] H. Liu et al. (E895 Collaboration), Nucl. Phys. A **638**, 451c (1998)
- [32] P.K. Sahu, W. Cassing, U. Mosel and A. Ohnishi, Nucl. Phys. A **672**, 376 (2000)
- [33] P. Crochet et al. (FOPI Collaboration), Nucl. Phys. A **624**, 755 (1997)
- [34] M.M. Htun et al., Phys. Rev. C **59**, 336 (1999)
- [35] M. Gyulassy, K.A. Frankel and H. Stöcker, Phys. Lett. B **110**, 185 (1982)
- [36] H. Gutbrod et al., Phys. Lett. B **216**, 267 (1989); Phys. Rev. C **42**, 640 (1990)

[37] D. Lambrecht et al., Z. Phys. A **350**, 115 (1994)

**Table 1.** Parameters sets for the different mean fields employed in the BUU calculation.

Not.	K (MeV)	$m^*/m_0$	A (MeV)	B (MeV)	C (MeV)	$\tau$	$\Lambda$ (fm $^{-1}$ )
H	380	1.00	-124.3	71.0	0.0	2.00	-
HM	379	0.68	-10.0	38.0	-63.6	2.40	2.13
HM1	379	0.62	22.2	29.5	-82.7	2.62	2.13
SM	220	0.68	-108.6	136.8	-63.6	1.26	2.13

## FIGURE CAPTIONS

- Fig. 1** Density dependence of the energy per nucleon in nuclear matter (upper left panel). The other three panels show the mean-field potential vs. momentum at the nuclear densities  $0.5\rho_0$ ,  $\rho_0$  and  $2\rho_0$ . The dashed, dotted, solid and dash-dotted lines correspond to the interactions H, HM, HM1 and SM, respectively.
- Fig. 2** Central baryon density (smooth lines) and NN collision rate (histograms) vs. time for Au+Au at 0.4 AGeV and  $b = 6$  fm. The solid (dashed) line and histogram correspond the HM (SM) calculation. The dotted line shows the normal nuclear density  $\rho_0$  for comparison.
- Fig. 3** Average transverse velocity (a) and transverse momentum (b) of neutrons in the c.m. rapidity range  $|y| < 0.1$  emitted in the reaction plane ( $\phi = -30^\circ \div 30^\circ$ ,  $150^\circ \div 180^\circ$ ,  $-180^\circ \div -150^\circ$ ) and out of the reaction plane ( $\phi = 60^\circ \div 120^\circ$ ,  $-60^\circ \div -120^\circ$ ) for Au+Au at 400 AMeV and  $b = 6$  fm.
- Fig. 4** Time evolution of the baryon density in the reaction plane  $(x, z)$  for Au+Au at 0.4 AGeV and  $b = 6$  fm. Isolines from outer to inner correspond to densities in the order 0.05, 0.1, 0.15, 0.20 and  $0.25 \text{ fm}^{-3}$ .
- Fig. 5** (a) Azimuthal dependence of the average neutron velocity and (b) neutron azimuthal distribution for Au+Au at 0.4 AGeV and  $b = 5 \div 7$  fm. Neutrons are selected in the c.m. rapidity interval  $|y| < 0.1$ . The corresponding elliptic flows are:  $v_2 = -0.046$  (H) and  $v_2 = -0.090$  (HM).
- Fig. 6** The elliptic flow  $v_2$  vs. transverse velocity (left panels) and vs. transverse momentum (right panels) of neutrons in the c.m. rapidity interval  $|y| < 0.1$  for the time steps  $t = 30 \text{ fm}/c$  (upper panels) and  $t = 50 \text{ fm}/c$  (lower panels). The calculations have been performed with the H (open circles, dashed line) and HM (full circles, solid line) parametersets. The system is Au+Au at 0.4 AGeV and  $b = 6$  fm.

**Fig. 7** Excitation function of the elliptic flow  $v_2$  as given by the collection of experimental data from various groups [30] and by the BUU calculations. The BUU curves are shown for Au+Au collisions at  $b = 5 \div 7$  fm for *free* (unbound) protons with a critical distance  $d_c = 3$  fm in the c.m. rapidity range  $|y| < 0.1$  (see text). The curves correspond to various mean-field parametersets. Upper panel: short-dashed – H, dash-dotted – SM, dotted – HM. Lower panel: dotted – HM, thick solid – HM1, long-dashed – HM1 with reduced (by 30%) NN cross section. For the reference the results of the cascade calculation without mean field are shown by thin solid line on the upper panel.

**Fig. 8** Excitation function of the transverse in-plane flow  $F$  for Au+Au collisions in comparison to the experimental data of the EOS, FOPI and E895 Collaborations as collected in Ref. [31]. The BUU curves on the upper and lower panels are marked as in Fig. 7. The BUU results are impact parameter weighted in the interval  $b = 5 \div 7$  fm and are obtained for *free* (unbound) protons with a critical distance  $d_c = 3$  fm in the rapidity range  $-0.2 < (y/y_p)_{c.m.} < 0.3$  (see text).

**Fig. 9** Azimuthal distributions of neutrons with respect to the flow axis ( $\phi'$ ) for collisions of Nb+Nb and La+La at 0.4 AGeV in comparison to the data (histograms) from Ref. [34]. Solid and dashed lines correspond to BUU calculations with HM1 and HM mean-field parametrizations, respectively. The BUU results are weighted in the impact parameter range  $b = 1 \div 5$  fm (Nb+Nb) and  $b = 1 \div 6$  fm (La+La) according to the estimate  $b_{max} = 0.5(R_p + R_t)$  in [34]. In the calculations we selected *free* neutrons ( $d_c = 3$  fm) with longitudinal momenta  $-0.1 \leq (p'_z/p'_{proj})_{c.m.} \leq 0.1$ .

**Fig. 10** Average neutron transverse in-plane momentum vs. normalized c.m. rapidity for Nb+Nb and La+La collisions at 0.4 AGeV in comparison to the data from [34]. The BUU results are weighted in the impact parameter range  $b = 1 \div 5$  fm (Nb+Nb) and  $b = 1 \div 6$  fm (La+La); free neutrons with a critical distance  $d_c = 3$  fm are selected in BUU. The solid and dashed lines correspond to the HM1 and HM parametrizations.

The experimental threshold laboratory kin. energy of 55 MeV for neutrons [34] is taken into account which leads to the asymmetric  $\langle p_x \rangle(y^{(0)})$ -dependence with respect to  $y^{(0)} = 0$ .

**Fig. 11** The neutron squeeze-out ratio  $R_N$  vs. impact parameter  $b$  for Au+Au collisions at 400 AMeV. The data from Ref. [37] are for neutrons in the rapidity interval  $0.4 \leq y/y_p < 0.6$ . The histograms represent BUU calculations with various mean-field parametersets. Upper panel: short-dashed – H, dash-dotted – SM. Lower panel: dotted – HM, solid – HM1. In BUU free neutrons are selected with  $d_c = 3$  fm and the angular cuts of the LAND detector are taken into account. The calculated azimuthal distributions are shown with respect to the reaction plane given by the  $\mathbf{Q}$  vector (see text).

**Fig. 12** Squeeze-out ratio of neutrons  $R_N$  in the rapidity interval  $0.4 \leq y/y_p < 0.6$  as a function of the neutron transverse momentum for collisions of Au+Au at 400, 600 and 800 AMeV. The data are from Ref. [37]; the histograms show the BUU calculations for different mean fields: short-dashed – H, dotted – HM, solid – HM1, dash-dotted – SM, long-dashed – HM1 with reduced (by 30%) NN cross section. The BUU results are impact parameter weighted in the region  $b = 5 \div 9$  fm, which approximately corresponds to the centrality bin E2 for the data. In the calculations the reaction plane was determined by the  $\mathbf{Q}$  vector.

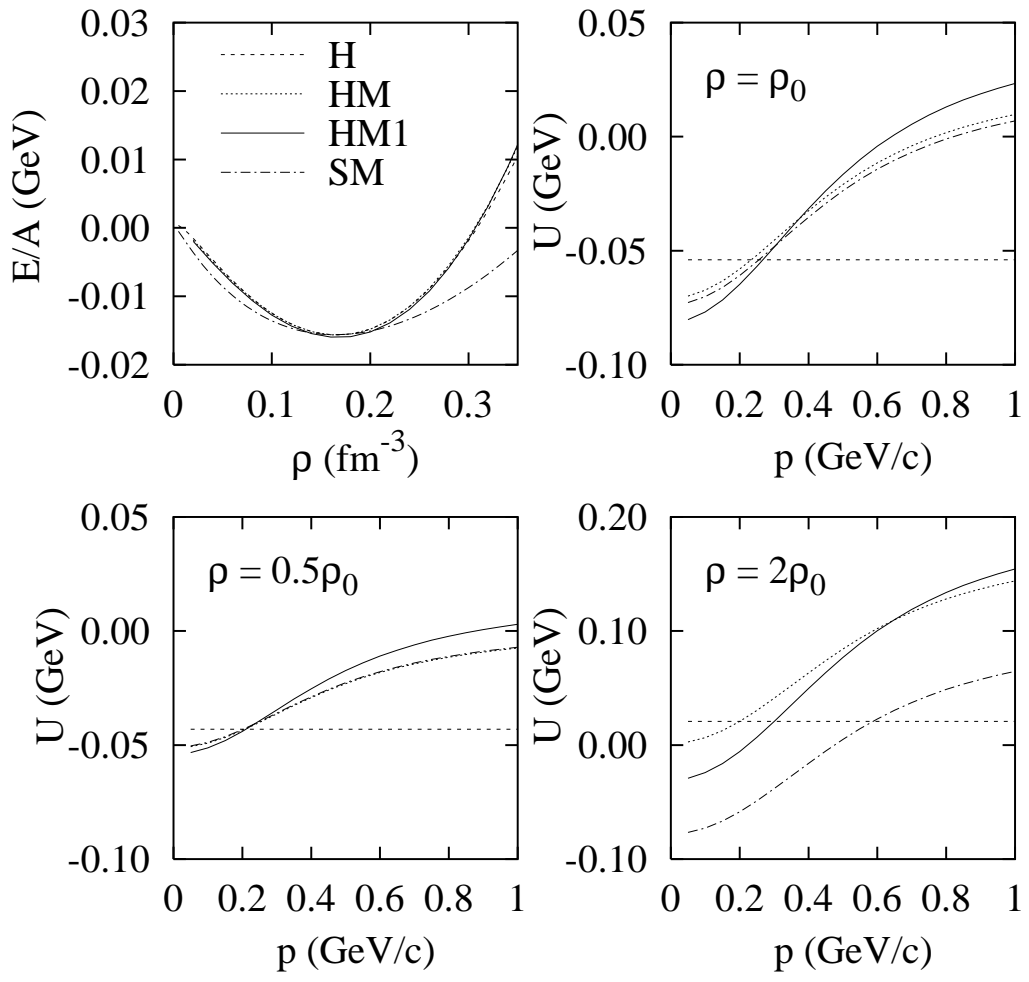


FIG. 1.

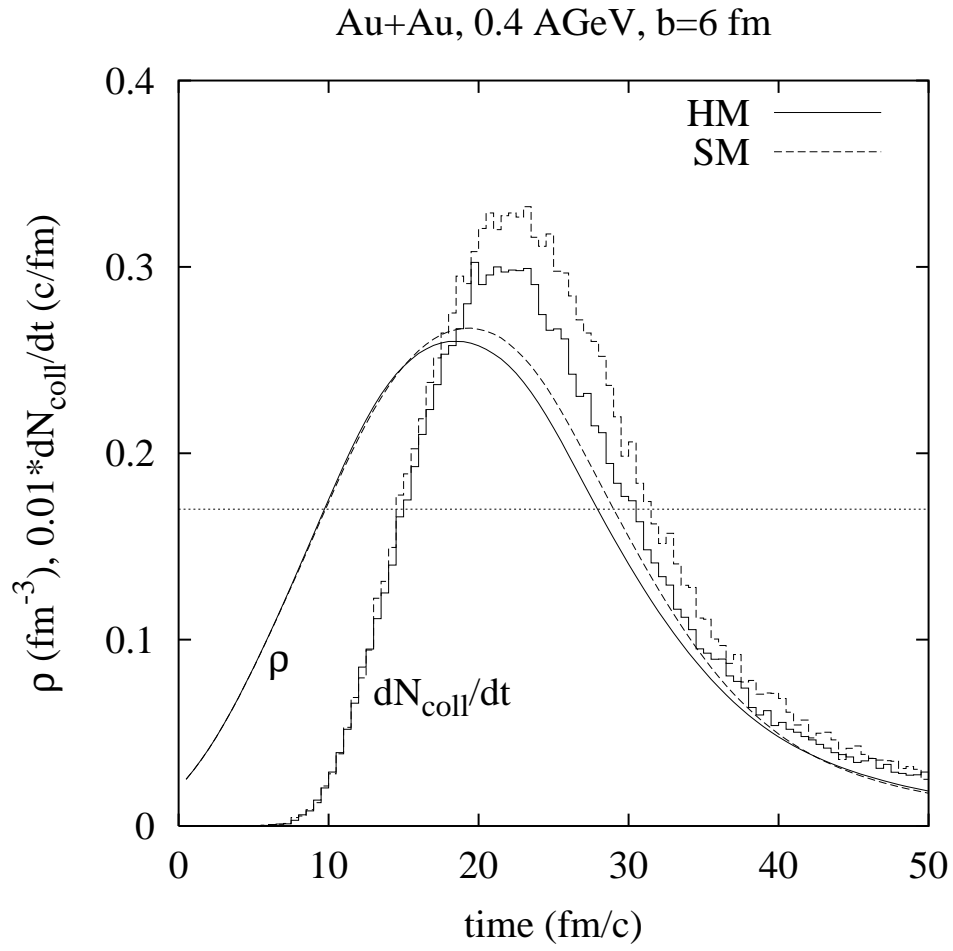


FIG. 2.

Au+Au, 400 AMeV, b=6 fm

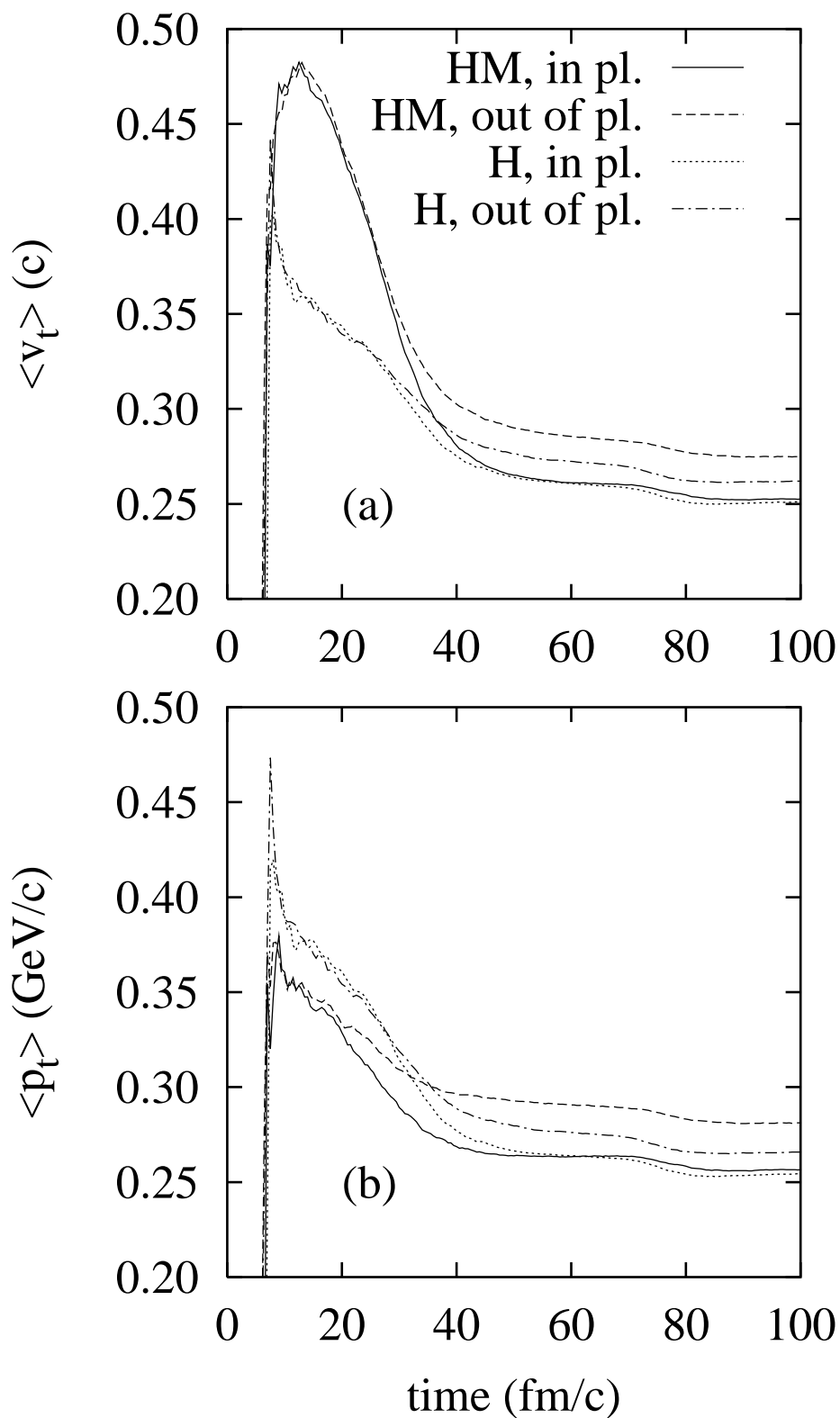


FIG. 3.

Au+Au, 0.4 AGeV, b=6 fm, HM

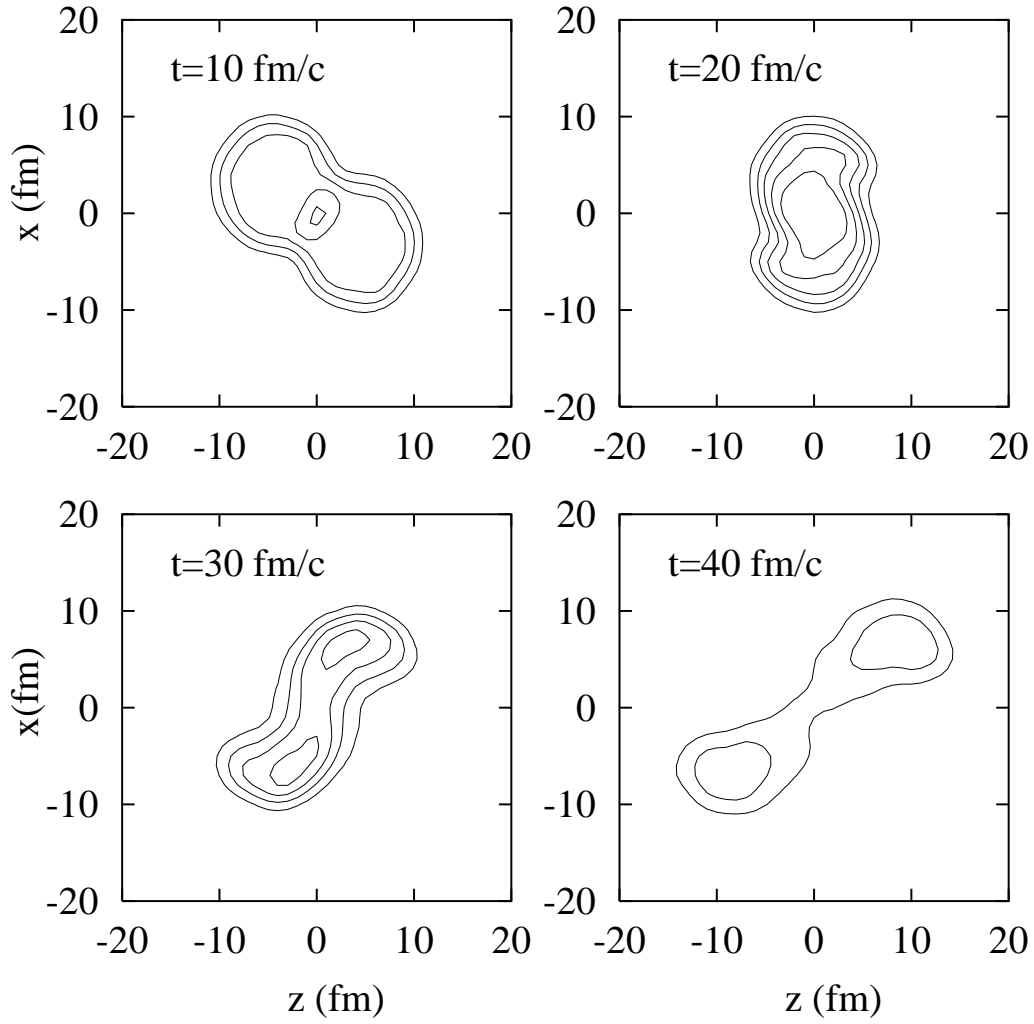


FIG. 4.

Au+Au, 0.4 AGeV, b=5-7 fm, neutrons

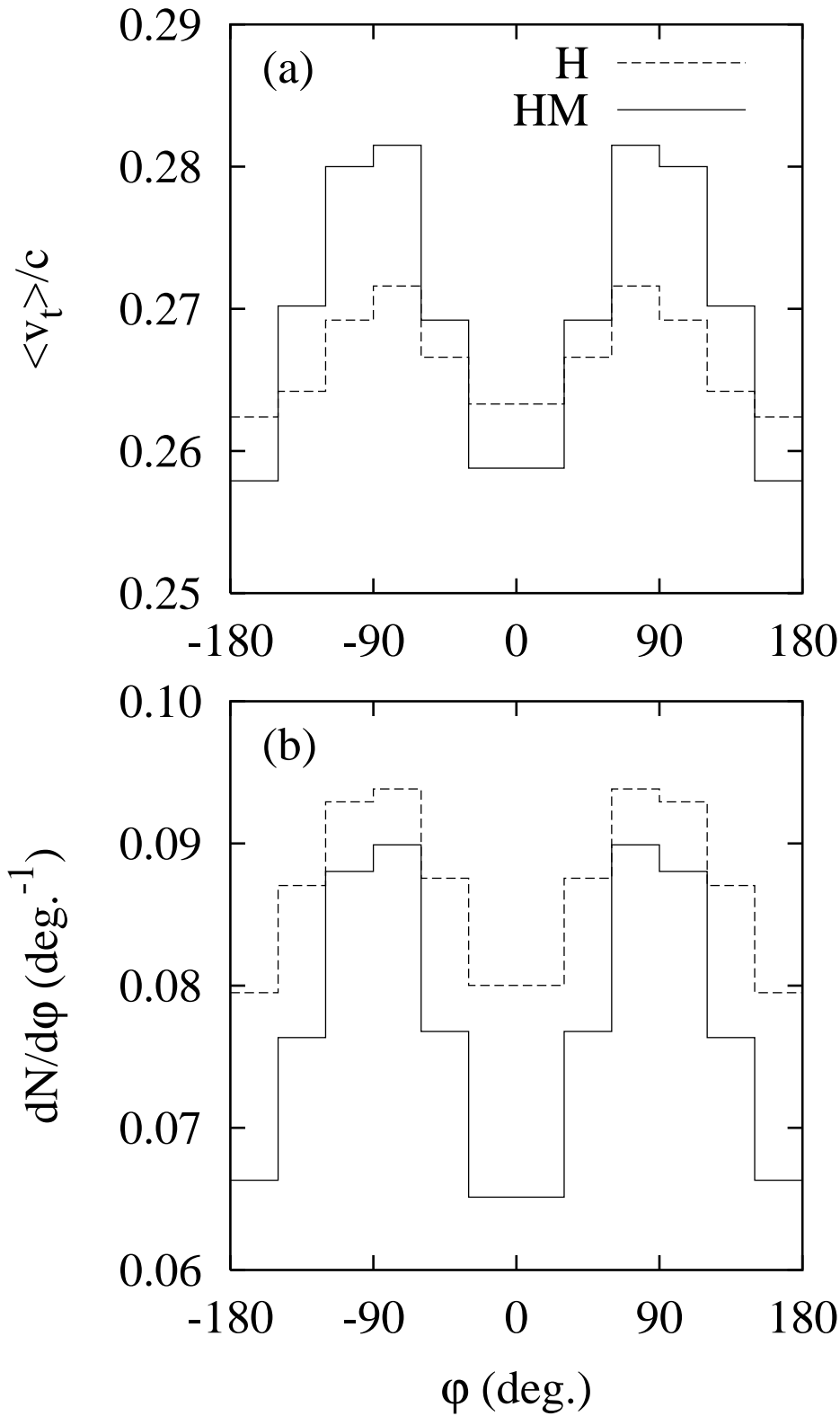


FIG. 5.

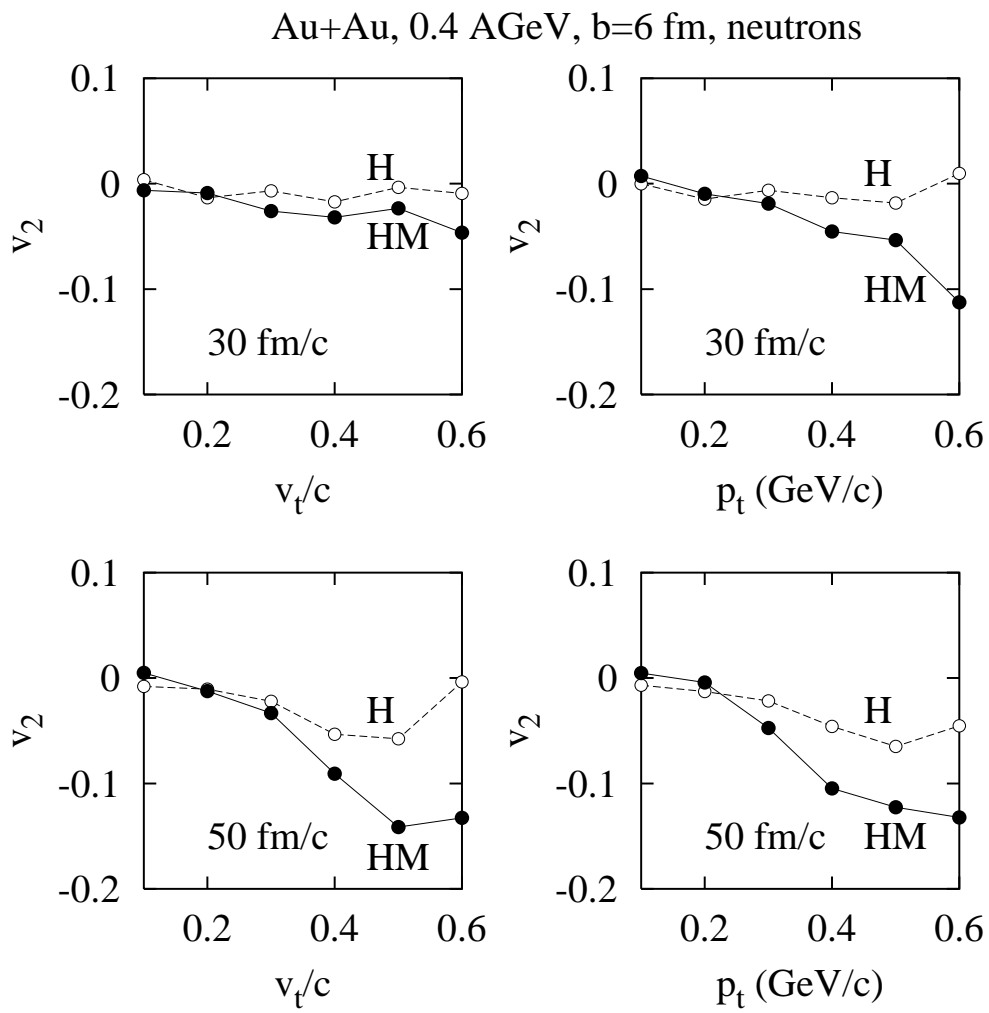


FIG. 6.

Au+Au, protons at midrapidity

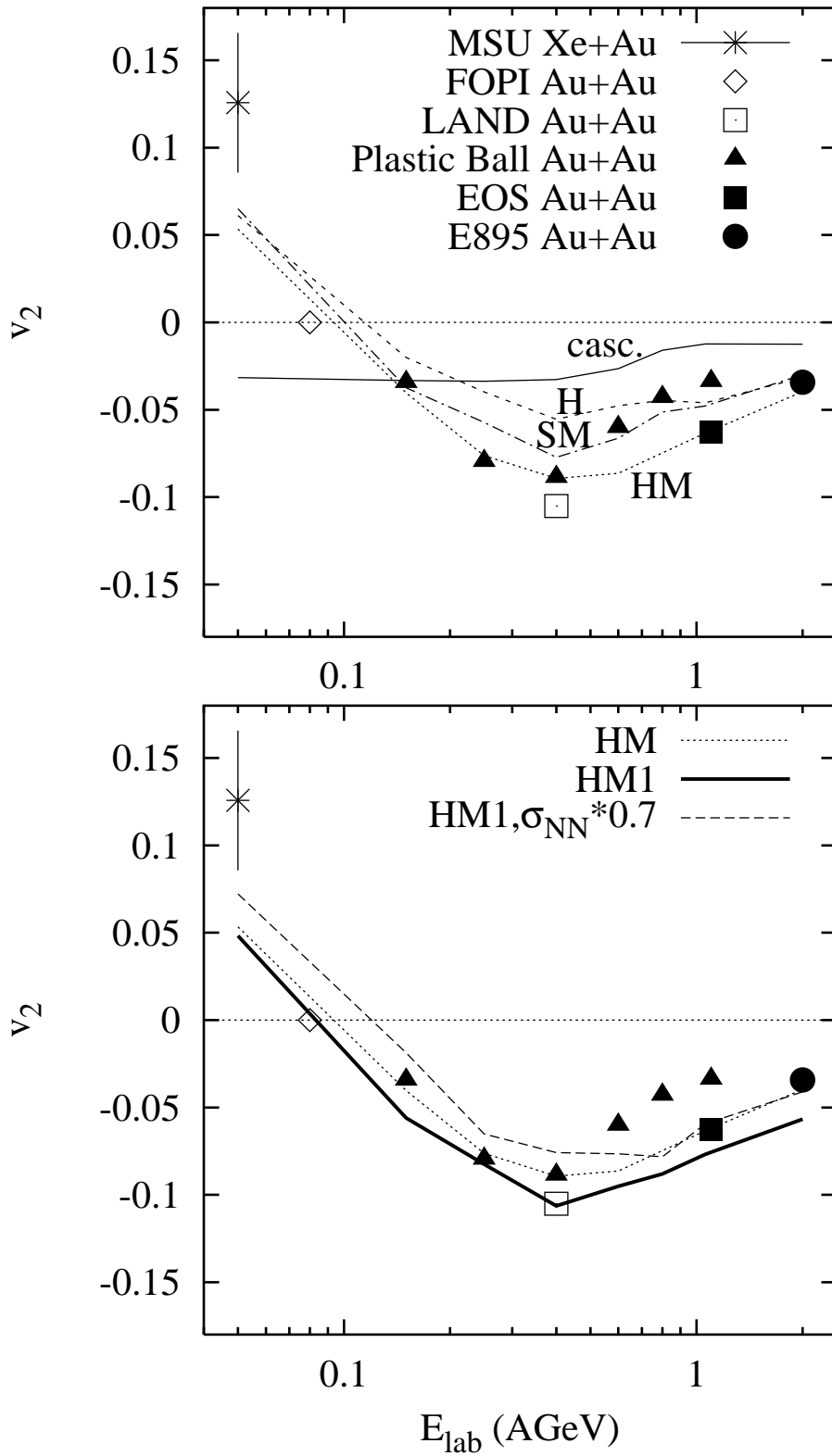


FIG. 7.

Au+Au, protons at midrapidity

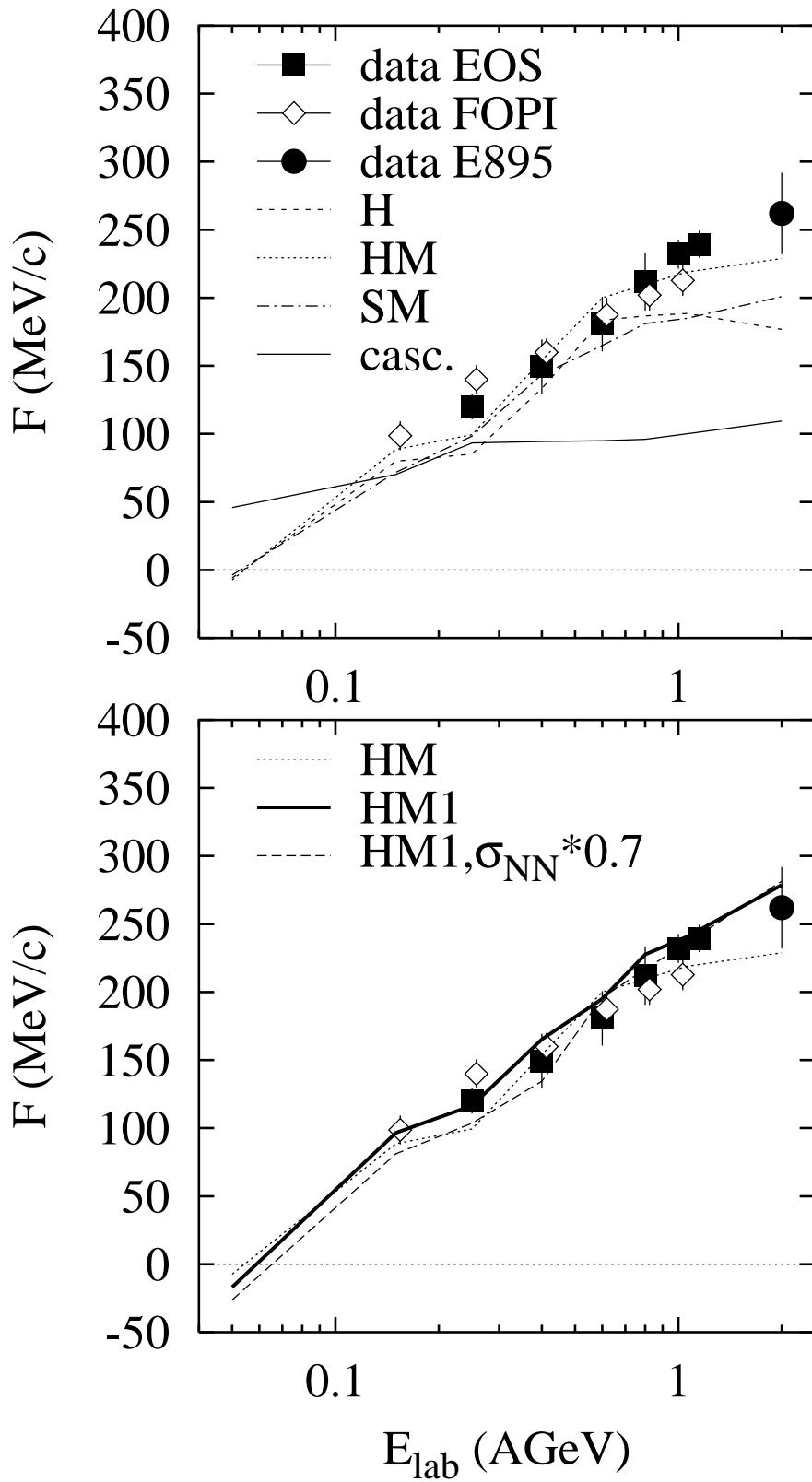


FIG. 8.

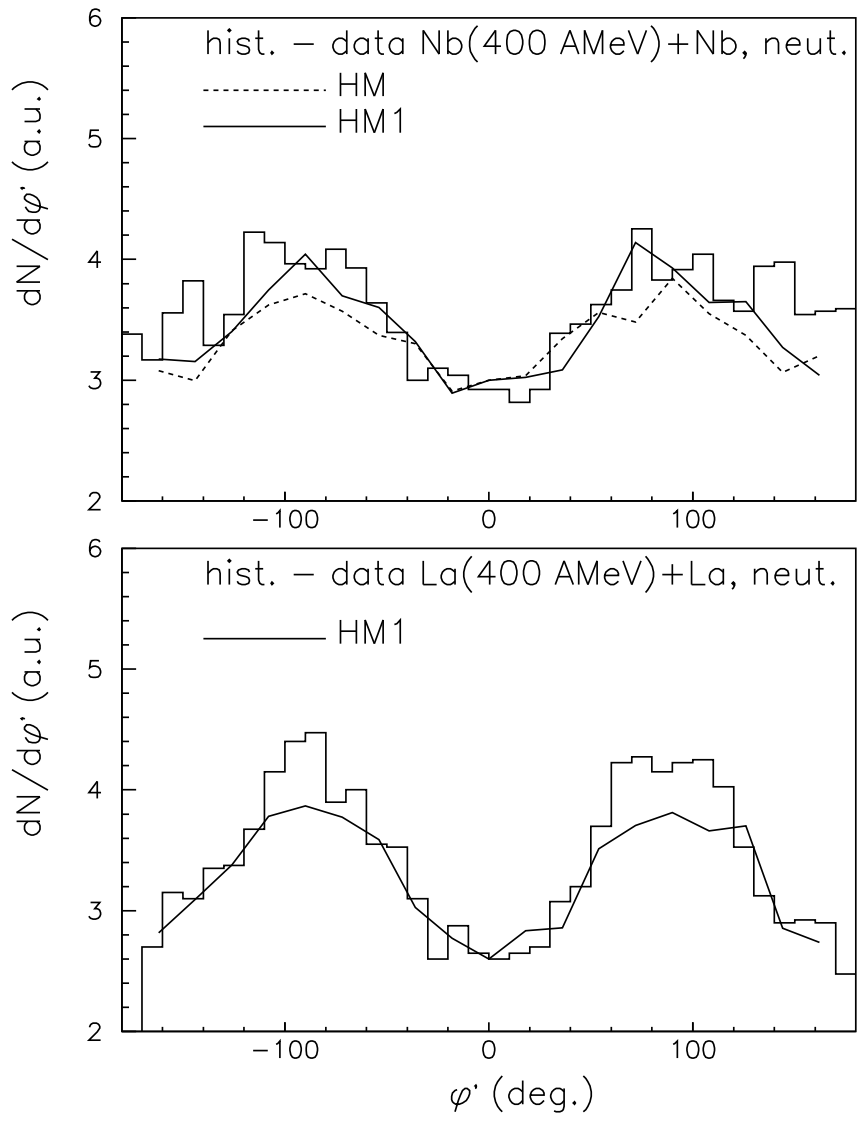


FIG. 9.

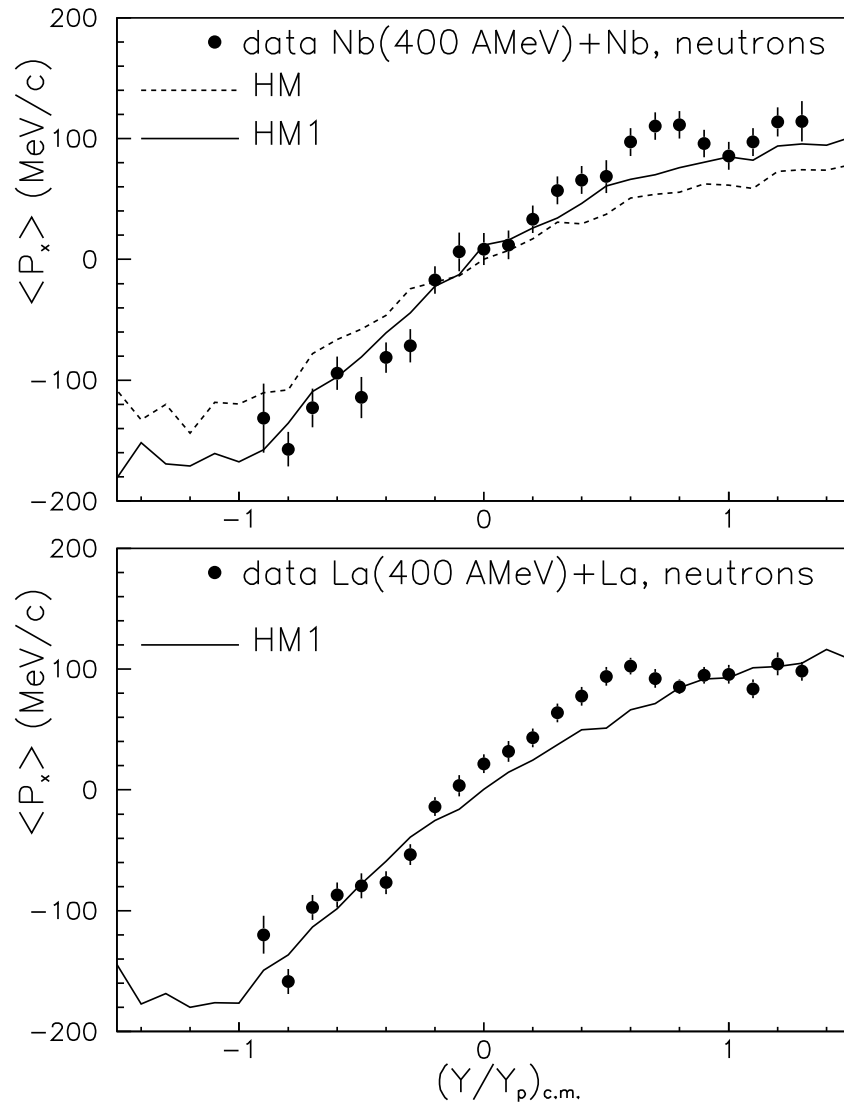


FIG. 10.

Au+Au, 400 AMeV, neutrons

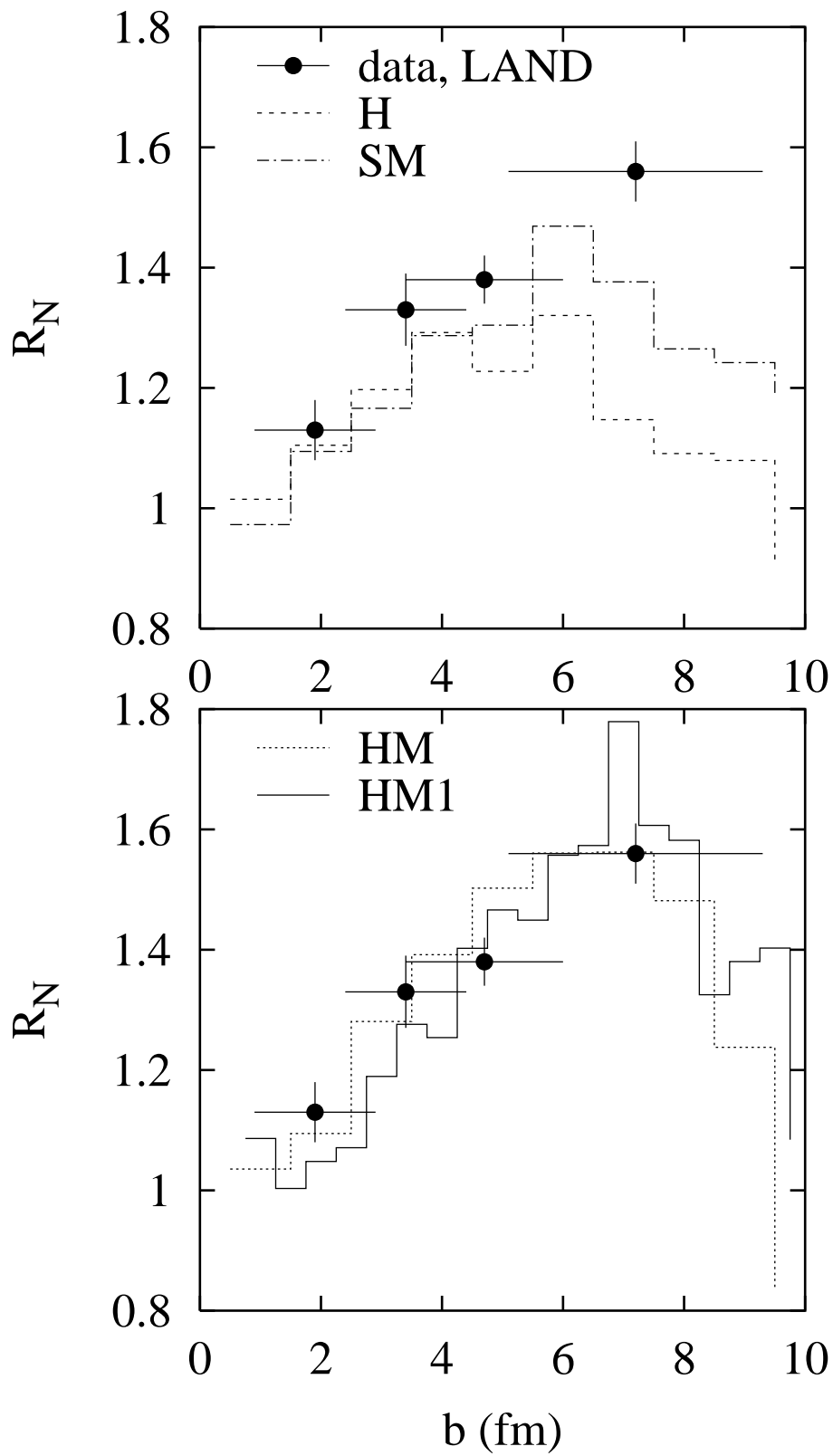


FIG. 11.

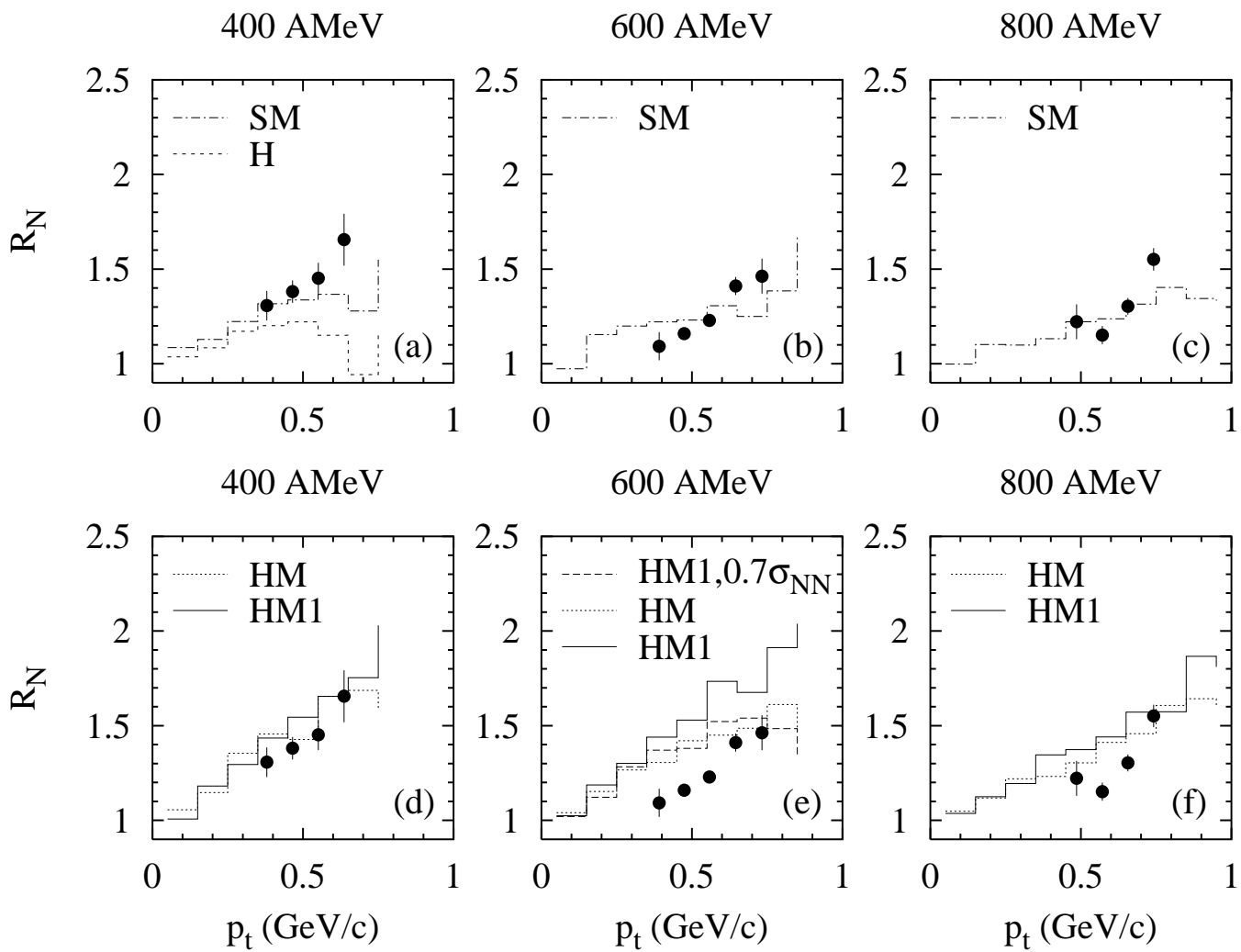


FIG. 12.